Industrial Chemistry & Materials

ROYAL SOCIETY OF CHEMISTRY

PAPER

View Article Online
View Journal

Cite this: DOI: 10.1039/d5im00114e

Design and construction of homogeneous heterogeneity Co–Zn-ZIF-L membranes for efficient H_2/CO_2 separation

Shenzhen Cong,†[a] Si Sun,†[a] Yijing Zhang,[a] Ming Wang,[a] Zhehua Jia,[a] Jiaoyu Peng*[b] and Huan Pang *[a]

Received 23rd June 2025,
Accepted 4th September 2025

DOI: 10.1039/d5im00114e

rsc.li/icm

Metal–organic framework (MOF) membranes have been extensively researched as an innovative membrane material for H_2/CO_2 separation. The preparation of MOF membranes can be extended by constructing MOF membranes with homogeneous heterogeneous structure and the MOF membranes with high permeance and high selectivity can be prepared. Here, we use the chelation-assisted interfacial growth process to construct a seeding layer, and then prepare Co–Zn-ZIF-L membranes with a homogeneous heterogeneous structure by secondary growth for the efficient separation of H_2/CO_2. The resulting Co–Zn-ZIF-L membranes show an H_2 permeance of 2156 GPU and H_2/CO_2 selectivity of 31.6 at 298 K and 1.0 bar, surpassing the Robeson upper bound (2008). Furthermore, the Co–Zn-ZIF-L membrane has a H_2/CO_2 separation stability of 65 h and can efficiently separate to obtain pure H_2.

Keywords: ZIF-L membrane; Oriented growth; H_2/CO_2 separation; Gas separation.

1 Introduction

Hydrogen (H_2) is an important industrial gas and has already occupied a significant position in industries.[1] Currently, H_2 in industry is primarily derived from the water-gas shift process of fossil fuels. However, the water-gas shift process produces a substantial amount of CO_2, low concentration of CO, trace H_2S, and so forth, which is insufficient to meet industrial requirements.[2] H_2 purification typically necessitates a significant investment in the separation process as well as running expenditures, raising the price of hydrogen significantly. Therefore, it is vital to explore an efficient and low-cost H_2 separation process.[3] The benefits of membrane-based separation technology, including its low cost, ease of preparation, and high separation efficiency,[4–6] have drawn the attention of researchers in addition to more conventional separation techniques like cryogenic distillation,[7] pressure swing adsorption (PSA),[7] and chemical adsorption.[8] Theoretically, membrane-based separation based on the dissolution–diffusion mechanism or size sieving is feasible because H_2 and CO_2 have similar dynamic diameters (H_2: 2.9 Å, CO_2: 3.3 Å),[9] but they differ greatly in polarity (CO_2 is a polar molecule, and H_2 is a non-polar molecule).[10] Although inorganic membranes have excellent thermal stability, their brittleness and high manufacturing cost limit large-scale application.[11] Polymeric membranes are susceptible to the trade-off effect,[12] which results in decreased selectivity. Consequently, a focal point of study in this domain is the development of innovative membrane materials characterized by elevated permeance, superior selectivity, and operational durability.

Metal–organic frameworks (MOFs) can be categorized as a type of crystalline porous materials that possess periodic network configurations, tunable pore size, functional structure and excellent specific surface area and have been widely used in gas storage and separation,[13,14] catalysis,[15] sensing[16] *etc.* Zeolitic imidazolate frameworks (ZIFs), a category of MOFs, have garnered significant interest owing to their structural similarity and superior stability compared to inorganic zeolite materials.[17] ZIFs are self-assembled by transition metal ions (such as Zn^{2+}, Co^{2+}) and imidazole ligands. Their topological structure is similar to that of traditional zeolites, but they have more flexible pore size control capabilities and excellent chemical stability.[18] The crystal structure of ZIF-L is different from the cubic topology of traditional three-dimensional zeolites but is stacked in a two-dimensional layered form.[19] Its basic structural unit is a tetrahedral structure formed by the coordination of metal

[a] School of Chemistry and Chemical Engineering, Yangzhou University, Yangzhou, 225009, China. E-mail: panghuan@yzu.edu.cn
[b] Key Laboratory of Green and High-end Utilization of Salt Lake Resources, Qinghai Engineering and Technology Research Center of Comprehensive Utilization of Salt Lake Resources, Qinghai Institute of Salt Lakes, Chinese Academy of Sciences, Xining 810008, China. E-mail: pengjy@isl.ac.cn
† These authors contributed equally to this work.

ions (Zn^{2+} or Co^{2+}) with four imidazole ligands, but these tetrahedrons form a layered network by sharing ligands. ZIF-L has two pore structures: interlayer confined channels formed by stacking between adjacent layers and six-membered ring windows formed by imidazole rings within the layers. The pore size of the interlayer confined channels is about 0.3 nm, which is close to the molecular size of H_2 and CO_2, and is suitable for separation based on molecular sieving effects. The pore size of the six-membered ring window formed by imidazole rings within the layer is about 0.4 nm, which can be used as a channel for rapid gas diffusion.[20] However, single-metal ZIF-L membranes continue to have issues such as high pore stiffness and a single chemical environment, limiting further progress in separation performance. To overcome the performance bottleneck of single-metal ZIF materials, researchers have advocated synergistically optimizing the membrane's pore size, surface chemistry, and mechanical properties by the use of heterostructure ZIF systems.[21]

The most frequent approach for creating heterostructures is heteroepitaxial growth.[22] Heteroepitaxial development is a useful approach for designing the properties of crystalline materials by integrating distinct crystal systems *via* molecular-level interactions. Unlike other MOF modification strategies (such as metal/ligand exchange and covalent/click chemistry on ligand side chain groups), this method of connecting two different crystal systems at the molecular level can produce mixed crystals with combined properties while preserving the intrinsic properties of individual crystals.[23] This distinct advantage of heteroepitaxial growth allows us to generate a sequence of multi-level MOF structures that cannot be obtained by other means.[24,25] It is worth noting that some zeolite films and membranes are made using heteroepitaxial growth methods.[26,27] Co-ZIF-L replaces the Zn^{2+} in ZIF-L with Co^{2+}, but the crystal structure remains the same. Furthermore, cobalt ions have a better coordination effect with dimethylimidazole, which can significantly improve the H_2/CO_2 separation performance of ZIF-L.[28,29]

The formation of crystals may be successfully controlled and the binding force between the MOF membrane and the support improved by network cross-linking chelated metal ions to aid in the diffusion growth of the interface.[30] In this work, polyvinyl alcohol (PVA) and polyallylamine (PAH) were used to cross-link chelated zinc ions, and the ZIF-L seed layer was constructed by diffusion growth at the interface, followed by secondary growth to fabricate a homogeneous heterostructure Co–Zn-ZIF-L membrane with high permeance and H_2/CO_2 separation selectivity. The arrangement and orientation of the ZIF-L membrane were altered by optimizing the polymer layer and regulating the growth orientation, and the effects of various circumstances on H_2/CO_2 selectivity and surface morphology were evaluated (Fig. 1).

2 Results and discussion

The poor contact between ZIF-L and the PSf support makes it challenging to develop ZIF-L membranes directly on the PSf support. The ZIF-L seeding layer was constructed by interfacial diffusion assisted by PVA–PAH chelated Zn^{2+}, and a continuous, defect-free homogeneous heterostructure Co–Zn-ZIF-L membrane was prepared by secondary growth on the Zn-ZIF-L surface by using an epitaxial growth strategy. PVA and PAH network cross-linking was used to chelate Zn^{2+} to prepare a PVA–PAH–Zn membrane with a smooth surface and low roughness (Fig. S2 and S3). The ZIF-L membrane prepared by *in situ* growth does not show selective absence of peaks and showed no obvious orientation growth (Fig. S4 and S5). The polymer network's adhesion and cross-linking capabilities limit metal ion and ligand diffusion, allowing ZIF-L nanosheets to form in an orderly manner at the interface. The cross-linked polymer covers surface imperfections in the support, producing homogeneous nucleation sites for secondary growth. The polymer's active groups ($-NH_2$, –OH) establish hydrogen or coordination

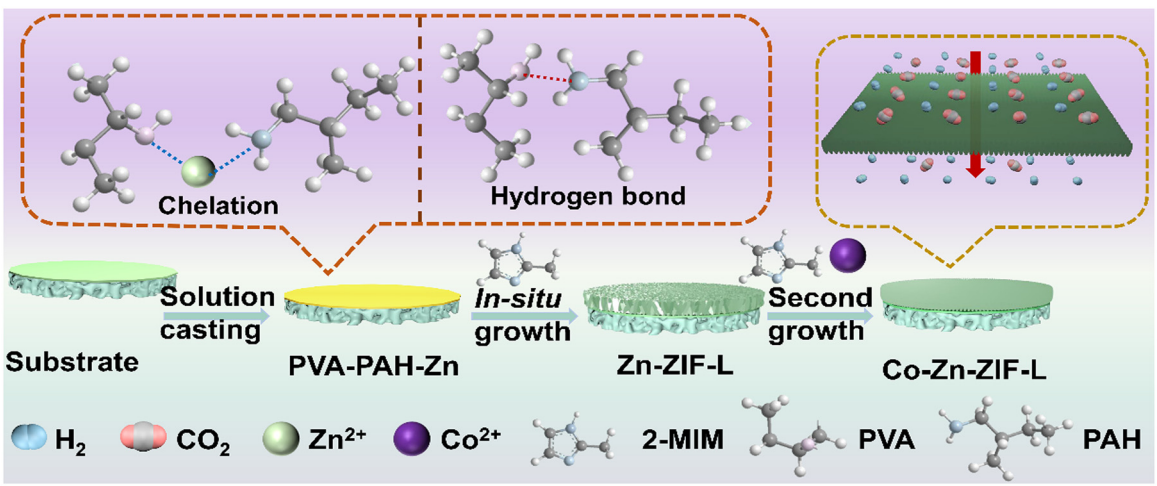

Fig. 1 Schematic of the preparation of the Co–Zn-ZIF-L membrane.

bonds with the support and ZIF-L, which improves membrane adherence. The polymer network creates a dense and aligned ZIF-L seed layer with the (100) crystal plane parallel to the carrier surface. This exposes lateral two-dimensional pores and creates an initial sieving path for H_2/CO_2. The thickness of the resulting Zn-ZIF-L membrane was approximately 1 μm and the surface roughness of the Zn-ZIF-L membrane increased (Fig. S4 and S6). The homogeneous heterostructure Co–Zn-ZIF-L membrane with obvious preferential orientation was prepared by epitaxial diffusion secondary growth and the thickness of the resulting membrane is approximately 1.7 μm (Fig. 2a and b and S7). Secondary growth fills the intercrystalline defects in the initial layer, resulting in a continuous, defect-free membrane structure. Co-introduction enhances the pore electron distribution of Zn-ZIF-L, boosting the preferential adsorption and diffusion of H_2 while also achieving molecular sieving through the pores. The XRD results of the Co–Zn-ZIF-L membrane showed a relatively strong peak at 2θ of 29.55° and a relatively weak peak at 2θ of 14.10°. These peaks correspond to the (800) and (400) crystal planes, respectively. The significantly higher intensity of the (800) crystal plane indicated the preferential *a*-axis orientation of the Co–Zn-ZIF-L membrane (Fig. 2c). By comparing the XRD patterns of the PAH-assisted membranes prepared *via in situ* growth and secondary growth, it can be observed that the PAH–Co–Zn-ZIF-L membrane expanded along the (112) and (800) crystal planes (Fig. S13). It can be considered that the seed layer has an inductive influence on the secondary growth, allowing crystals to develop in the orientation direction.[31] Co–Zn-ZIF-L is synthesized *via* epitaxial diffusion growth on the surface of a Zn-ZIF-L membrane, but Co–Zn-ZIF-L has preferred orientation growth and the membrane surface is not continuously formed, resulting in a higher surface roughness than the Zn-ZIF-L membrane (Fig. 2d). The cross-sectional EDS results of the Co–Zn-ZIF-L membrane show that Zn, accounting for 7.13%, is mainly in the lower half of the membrane layer and Co, accounting for 20.07%, is mainly in the upper half of the membrane layer, indicating that a homogeneous heterogeneous structure Co–Zn-ZIF-L membrane has been successfully constructed (Fig. 2e, S14 and S15).

To investigate the influence of network cross-linked chelated metal-assisted interface diffusion on the membrane structure during the manufacture of the ZIF-L membrane, attenuated total reflection Fourier-transform infrared spectroscopy (ATR-FTIR) was used. The ATR-FTIR spectra of the PVA/PAH–Zn membrane revealed no discernible peak near 400 cm^{-1}, indicating that no clear coordination structure had formed at this point. However, the ATR-FTIR spectrum of the Zn-ZIF-L membrane revealed an evident but weak signal near 400 cm^{-1}, showing that the Zn–N coordination bond was formed initially. Following the second growth, the membrane thickness and peak intensity rose dramatically, indicating the development of Co–N and a more ordered ZIF-L structure (Fig. 3b). The ATR-FTIR spectra of resulting powders showed a similar peak augmentation pattern (Fig. 3a). We also performed ATR-FTIR analysis on PVA and PAH membranes, and the Zn–N/Co–N coordination peaks in the membranes followed the expected trend (Fig. S16 and S17). The ATR-FTIR spectra of the PVA/PAH–Zn membrane showed the characteristic peaks of both –OH and $–NH_2$, which further reflected the influence of network cross-linked chelated metal-assisted interface diffusion on the membrane structure during the manufacture of the ZIF-L membrane. The adsorption of H_2 and CO_2 on Co–Zn-ZIF-L powders at 303 K reveals that Co–Zn-ZIF-L has linear adsorption for H_2 and conventional Langmuir adsorption for CO_2 (Fig. 3c and d). The H_2

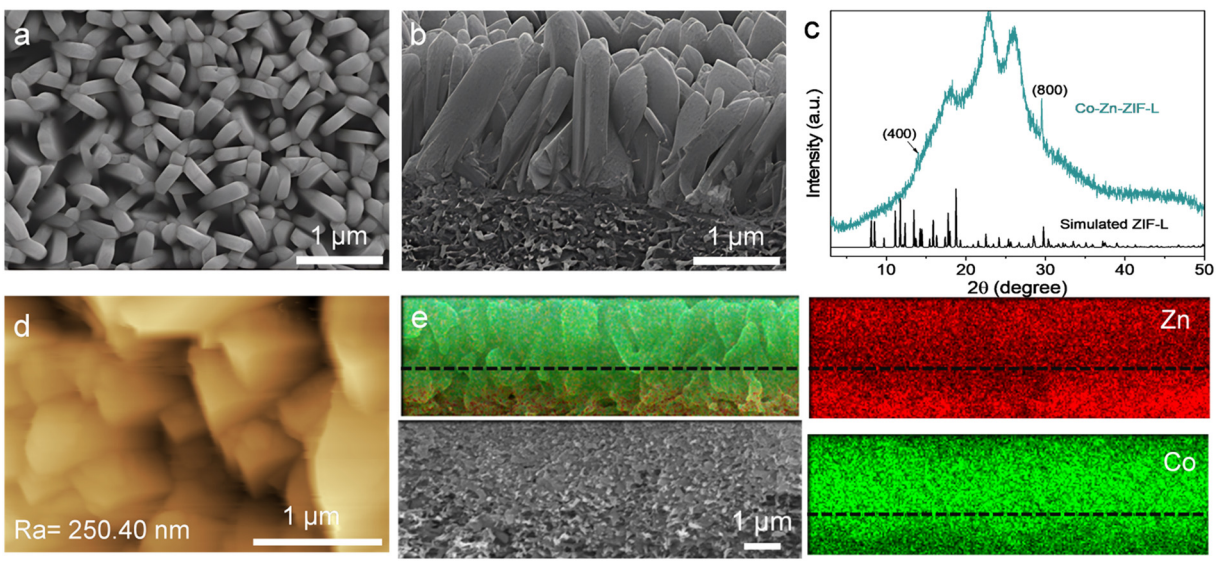

Fig. 2 Surface (a) and cross-sectional (b) SEM images of the Co–Zn-ZIF-L membrane. (c) Simulated and experimental XRD patterns of the Co–Zn-ZIF-L membrane. (d) AFM image of the Co–Zn-ZIF-L membrane. (e) EDS image of the Co–Zn-ZIF-L membrane.

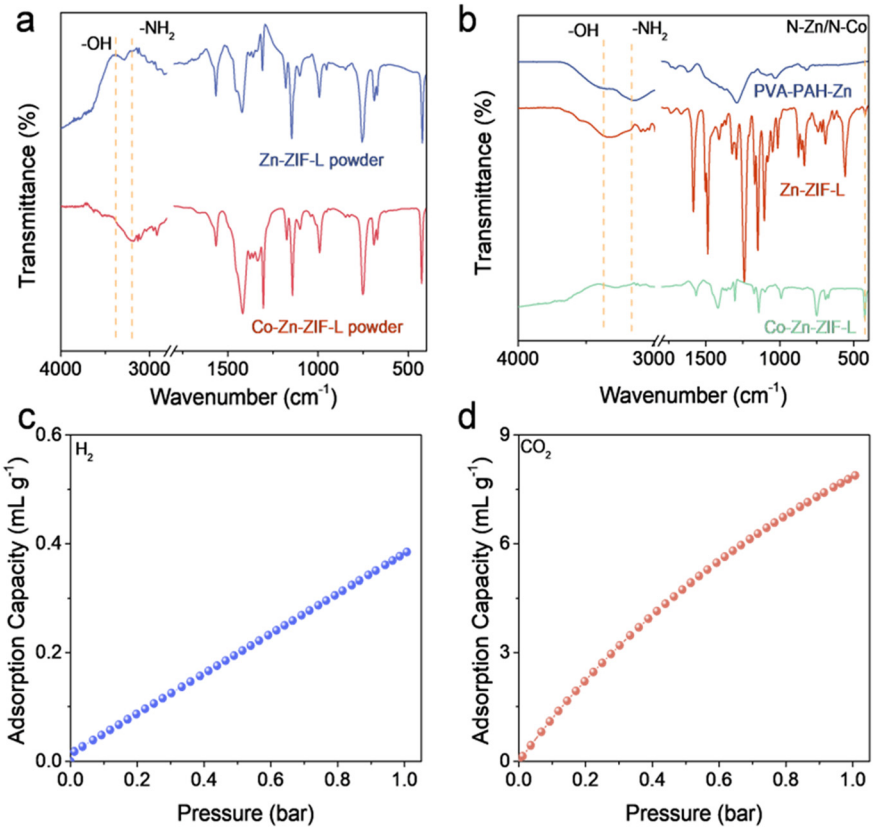

Fig. 3 (a) ATR-FTIR spectrum of Zn-ZIF-L and Co–Zn-ZIF-L powders; (b) ATR-FTIR spectrum of PVA–PAH–Zn, Zn-ZIF-L and Co–Zn-ZIF-L membranes; the adsorption isotherms of Co–Zn-ZIF-L powder for H_2 (c) and CO_2 (d) at 303 K.

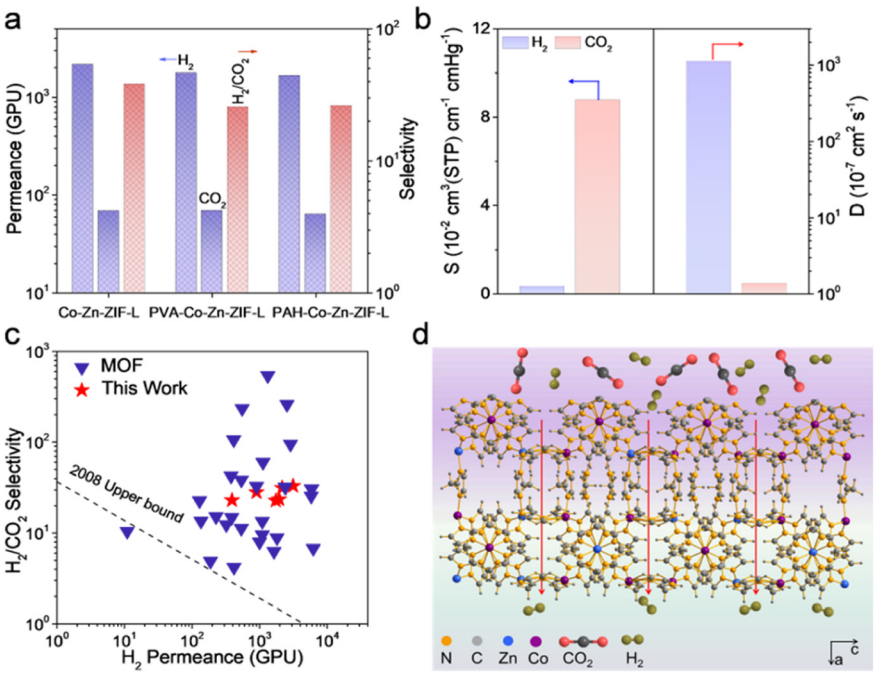

Fig. 4 (a) Gas permeance and H_2/CO_2 selectivity of resultant ZIF-L membranes. Feed pressure, 1.0 bar; temperature, 298 K; $H_2:CO_2$, 1 : 1. (b) Solubility coefficient and diffusion coefficient of the Co–Zn-ZIF-L membrane for H_2 and CO_2 (the Co–Zn-ZIF-L membrane thickness is 1.7 μm based on the cross section SEM). (c) The performance comparison of ZIF-L membranes in this work, the Robeson upper bound, and the ZIF-L membranes reported in previous literature (permeability was converted to a membrane thickness of 1 μm for the permeance). (d) Schematic of the H_2 and CO_2 molecules permeating the Co–Zn-ZIF-L framework along the *a*-axis.

molecule is small and can freely enter the microporous structure of Co–Zn-ZIF-L. The interaction with Co–Zn-ZIF-L is modest, resulting in linear adsorption. The CO_2 molecules are bigger and have a quadrupole moment. They can form monolayer chemical adsorption with open metal sites (*e.g.* Co^{2+}) or nitrogen-containing ligands in Co–Zn-ZIF-L by dipole–quadrupole or acid–base interactions, exhibiting typical Langmuir adsorption behaviour. This differential in adsorption gives Co–Zn-ZIF-L a high potential for H_2/CO_2 separation.

To acquire a better knowledge of the intercrystalline structure of the secondary generated Co–Zn-ZIF-L membrane, the prepared Co–Zn-ZIF-L membrane's H_2/CO_2 separation performance was evaluated by a Wicke–Kallenbach approach. The Co–Zn-ZIF-L membrane outperformed the PVA-Co–Zn-ZIF-L and PAH-Co–Zn-ZIF-L membranes in terms of H_2/CO_2 separation performance, with an H_2 permeance of 2156 GPU and an H_2/CO_2 selectivity of 31.6 (Fig. 4a). The separation performance of the constructed ZIF-L membrane surpassed the Robeson upper bound (2008), and when compared to H_2/CO_2 separation membranes described in the literature, the ZIF-L membrane showed potential advantages (Fig. 4c). The solubility coefficient and diffusion coefficient of H_2 and CO_2 in the Co–Zn-ZIF-L membrane were calculated to analyse the transport mechanism of H_2 and CO_2 in the Co–Zn-ZIF-L membrane (Fig. 4b). The adsorption of CO_2 by the ZIF-L framework is substantially higher than that of H_2, hence the CO_2 solubility coefficient of the Co–Zn-ZIF-L membrane is higher than that of H_2. The diffusion differential of H_2/CO_2 in the Co–Zn-ZIF-L membrane is the primary mechanism for H_2/CO_2 separation. Considering the analysis of the source of performance, we tested the separation performance of PVA/PAH–Zn, Zn-ZIF-L, and Co–Zn-ZIF-L membranes. The results demonstrated that the high separation performance of the Co–Zn-ZIF-L membrane stemmed from the ZIF-L structure with a porosity between that of H_2 and CO_2. Furthermore, directed development of ZIF-L along the *a*-axis is essential for successful H_2/CO_2 separation (Fig. 4d).[32]

The effect of feed temperature on the performance of the Co–Zn-ZIF-L membrane was evaluated (Fig. 5a). The permeance of the tested H_2 and CO_2 increased as the temperature improved, indicating that there is activated diffusion of gas molecules in the Co–Zn-ZIF-L framework. The changes in separation performance of the Co–Zn-ZIF-L membrane were studied under various pressure conditions. The permeance of H_2 and CO_2 reduced as pressure climbed (Fig. 5b). It is possible that Co–Zn-ZIF-L has a better adsorption capacity for CO_2. As the pressure rises, the amount of CO_2 adsorbed on the ZIF-L pores increases dramatically, occupying more diffusion sites and blocking H_2 permeation. The CO_2 permeance decreases due to adsorption saturation, but H_2 diffusion is significantly impeded, resulting in a loss of selectivity. H_2 purification requires a high level of membrane stability. In this investigation, the membrane's separation ability under dry and wet circumstances was assessed (Fig. 5c). During 65 h of continuous evaluation under dry conditions, the membrane maintained a nearly constant H_2 permeance (approximately 2100 GPU) and H_2/CO_2 selectivity (around 32). The addition of water vapor to the feed reduced the permeance of H_2 and CO_2. The water transport segment of the membrane used the H_2 and CO_2 channels. This blocking effect is more noticeable for larger CO_2 molecules, which increases the H_2/CO_2 selectivity. To verify the results,

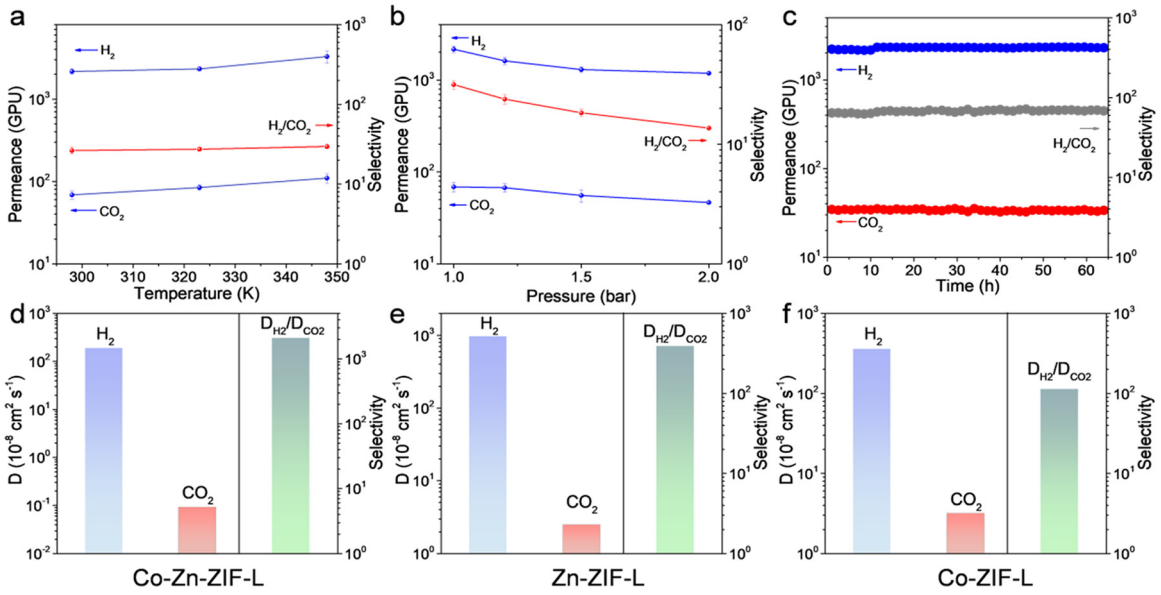

Fig. 5 The H_2/CO_2 separation performance of the Co–Zn-ZIF-L membrane at different operation temperatures (a) and pressures (b). (c) Operational stability of the Co–Zn-ZIF-L membrane for H_2/CO_2 separation. Feed pressure, 1.0 bar; temperature, 298 K; $H_2:CO_2$, 1 : 1. The diffusion coefficient of (d) Co–Zn-ZIF-L, (e) Zn-ZIF-L and (f) Co-ZIF-L for H_2 and CO_2 calculated by molecular dynamics simulation.

we performed molecular dynamics simulation (MDS) and diffusion coefficient tests on Co–Zn-ZIF-L powder. The study found that the diffusion coefficient of H_2 was significantly higher than that of CO_2, indicating that CO_2 encountered greater resistance when permeating the membrane layer (Fig. 5d–f). The Zn-ZIF-L membrane exhibited high flux but poor selectivity, which further confirmed the impact of the synergistic effect between Zn and Co bimetals on the membrane performance.

3 Conclusions

To achieve efficient H_2/CO_2 separation, the orientation growth of ZIF-L was regulated by polymer cross-linking coupling-assisted interfacial diffusion. A continuous, defect-free *a*-axis-oriented heterostructure Co–Zn-ZIF-L membrane was built on the surface of a porous substrate. This strategy effectively controlled the directional assembly and tight stacking of ZIF-L nanosheets at the interface by introducing a polymer cross-linking network, significantly inhibited the formation of non-selective defects, and improved the membrane layer's mechanical stability and interfacial bonding strength. The synthesized Co–Zn-ZIF-L membrane demonstrated superior H_2/CO_2 separation performance. The H_2 permeance reached 2156 GPU, while the H_2/CO_2 selectivity was as high as 31.6 at 298 K and 1.0 bar, far surpassing the Robeson upper bound (2008) and outperforming most reported ZIF-based separation membranes. Mechanistic studies have revealed that the synergistic action of Co and Zn improves the microenvironment of ZIF-L pores. The polymer cross-linking coupling-assisted interface diffusion control strategy creates an oriented growth dense membrane structure. This allows for rapid screening and transmission of H_2 molecules in sub-nanometer pores while effectively blocking CO_2 molecules through pore confinement and surface diffusion. This work not only gives new ideas for the green preparation of high-performance MOF membranes but also provides critical material support for boosting the development of efficient gas separation technology in the context of hydrogen economy and carbon neutrality.

4 Experimental section

4.1 Materials

Polyvinyl alcohol (PVA, M_w = 2–200 kDa, 99%), $Co(NO_3)_2{\cdot}6H_2O$ (99%), and 2-methylimidazole ($C_4H_6N_2$, 99%) were purchased from Aladdin Reagents (Shanghai) Co., Ltd. Polyacryl ammonium hydrochloride (PAH, M_w = 10–20 kDa) was obtained from Beijing Huawei Ruike Chemical Co., Ltd. $Zn(NO_3)_2{\cdot}6H_2O$ (99%) was purchased from Sinopharm Reagent Co., Ltd. Anhydrous ethanol was purchased from Hongbaoli (Beijing) Co., Ltd. Deionized water was made in the laboratory. All reagents were used without further purification.

4.2 The preparation of Co–Zn-ZIF-L membranes

4.2.1 Fabrication of Zn-ZIF-L membranes. To make a 4% PVA solution, PVA was mixed with water and refluxed and agitated for 12 h at 80 °C. PAH was added to water and agitated at room temperature for 30 min to produce a 4% PAH solution. Equal amounts of the PVA solution and PAH solution were mixed together to obtain a 2 wt% PVA/PAH solution. 2.97 g of $Zn(NO_3)_2{\cdot}6H_2O$ was added to 100 mL PVA/PAH solution, PVA solution and PAH solution to prepare PVA/PAH–Zn^{2+}, PVA–Zn^{2+} and PAH–Zn^{2+} solutions. The PVA/PAH–Zn^{2+} membrane layer was then prepared by applying a certain amount of PVA/PAH–Zn^{2+} solution to the Psf support and drying it at 50 °C for 12 h. Subsequently, the ZIF-L membrane was prepared by adding 2-MIM at a concentration of 0.8 mol L^{-1}, reacted for 2 h and washed with anhydrous ethanol several times. The PVA–ZIF-L and PAH–ZIF-L membranes were prepared using the same method.

4.2.2 Preparation of Co–Zn-ZIF-L membranes. The Co–Zn-ZIF-L membrane was fabricated by secondary growth, as follows: 1 mL of $Co(NO_3)_2{\cdot}6H_2O$ solution (0.1 mol L^{-1}) and 2 mL of 2-MIM solution (0.8 mol L^{-1}) were added to the previously made ZIF-L membrane and reacted for 4 h, followed by washing with sewage ethanol and drying to obtain a homogeneous heterogeneous Co–Zn-ZIF-L membrane. The PVA–Co–Zn-ZIF-L and PAH–Co–Zn-ZIF-L membranes were prepared using the same process.

4.2.3 Preparation of MOF powders. All MOF powders were extracted from the corresponding mother solutions after the fabrication of membranes, washed with ethanol by centrifugation and dried for further use.

4.3 Characterization

The morphology of the samples was observed by a scanning electron microscope (SEM, Zeiss_Supra55) under an acceleration voltage of 5.0 kV. EDS mapping images were captured on a Gemini 300 transmission electron microscope. The material's crystal structure was studied using X-ray diffraction (XRD) on a Bruker D8 Advanced X-ray diffractometer (Cu Kα radiation: λ = 0.154 nm). The ATR-FTIR spectrum of samples was recorded in the range of 500 to 4000 cm^{-1} on a Cary 610/670 FTIR spectrometer. AFM images were obtained from an SPM-9700HT atomic force microscope. The gas adsorption isotherms of ZIF-L powders were measured using the pressure decay method. The H_2 and CO_2 adsorption of ZIF-L powders was evaluated by a BSD-PM (PM2-1516-B) analyser at 303 K. The ZIF-L particles were activated at 120 °C for 24 h before the adsorption test.

4.4 Gas permeation experiments

The gas separation performance test was carried out at room temperature with H_2 and CO_2 having a feed flow rate of 30 mL min^{-1} respectively, and argon (99.99%) acting as the sweep gas with a flow rate of 20 mL min^{-1}. All the gases were purchased from Jiulong Company of Yangzhou. For the performance test, detection was performed using a Fuli

F70 gas chromatograph equipped with a highly sensitive thermal conductivity detector (TCD). The test process device is shown in Fig. S1.

Eqn (1) was employed to determine the gas permeance:

$$P_i = \frac{N_i}{\Delta p_i \cdot A} \quad (1)$$

where P_i (measured in mol m^{-2} s^{-1} Pa^{-1}), N_i (in mol s^{-1}) and Δp_i (Pa) represent the gas permeance of component i, its molar flow under standard state conditions, and the transmembrane pressure drop, respectively. A (m^2) designates the effective area of the membrane. For ease of comparison, gas permeance values are commonly converted to GPU units, with 1 GPU equivalent to 3.348×10^{-10} mol m^{-2} s^{-1} Pa^{-1}.

Eqn (2) was employed to determine the gas permeance:

$$\alpha_{H_2/CO_2} = \frac{P_{H_2}}{P_{CO_2}} \quad (2)$$

where P represents the gas permeance coefficients of H_2 and CO_2, calculated under identical experimental conditions, respectively.

Author contributions

S. C. and S. S. conceived the idea, designed the experiments, measured the H_2/CO_2 separation performance, interpreted the data, and wrote the paper. S. S. prepared membranes. Y. Z. and M. W. analysed the morphology of ZIF-L membranes. Z. J. and Y. Z. analysed the data. J. P. secured the funding and provided EDS line-scan test. H. P. supervised and secured the funding. All authors contributed to reviewing, editing, and revising the paper.

Conflicts of interest

The authors declare no conflict of interest.

Data availability

Supplementary information: The SI contains various characterization information. See DOI: **https://doi.org/10.1039/D5IM00114E**.

The authors support the data underlying the results reported in this paper, and all data are presented in the main text and SI.

Acknowledgements

This work was financially supported by the Project for International Cooperation in Science and Technology, Qinghai Province (No. 2024-HZ-804), the Yangzhou "Green Yang Jinfeng Plan" excellent doctor talent funding program and the Yangzhou University Startup Fund for Distinguished Scholars (137013525).

References

1 L. M. Germeshuizen and P. W. E. Blom, A techno-economic evaluation of the use of hydrogen in a steel production process, utilizing nuclear process heat, *Int. J. Hydrogen Energy*, 2013, **38**, 10671–10682.
2 S. P. Cardoso, I. S. Azenha, Z. Lin, I. Portugal, A. E. Rodrigues and C. M. Silva, Inorganic membranes for hydrogen separation, *Sep. Purif. Rev.*, 2018, **47**, 229–266.
3 C. Y. Chuah, J. Lee and T.-H. Bae, Graphene-based membranes for H_2 separation: Recent progress and future perspective, *Membranes*, 2020, **10**, 336.
4 J. Wang, C. Yuan, C. Li, G. Geng, J. Song, N. Yang, S. Kawi, J. Sunarso, X. Tan and S. Liu, Nickel-based metallic membranes for hydrogen production in membrane reactor: A brief overview, *Sep. Purif. Technol.*, 2024, **358**, 130435.
5 J. Fu, S. Das, G. Xing, T. Ben, V. Valtchev and S. Qiu, Fabrication of COF-MOF composite membranes and their highly selective separation of H_2/CO_2, *J. Am. Chem. Soc.*, 2016, **138**, 7673–7680.
6 M. Liu, J. Emery and R. Guo, Microporous pentiptycene-based polybenzimidazole membranes for high temperature H_2/CO_2 separation, *J. Membr. Sci.*, 2025, **718**, 123673.
7 Y. Ko, J.-H. Kang, H. Do, J. Kum and C.-H. Lee, Hybrid process using cryogenic and pressure swing adsorption process for CO_2 capture and extra H_2 production from a tail gas in a steam methane reforming plant, *Energy Convers. Manage.*, 2025, **328**, 119561.
8 L. F. A. S. Zafanelli, E. Aly, A. E. Rodrigues and J. A. C. Silva, A novel cryogenic fixed-bed adsorption apparatus for studying green hydrogen recovery from natural gas grids, *Sep. Purif. Technol.*, 2023, **307**, 122824.
9 Y. Peng, Y. Li, Y. Ban, H. Jin, W. Jiao, X. Liu and W. Yang, Metal-organic framework nanosheets as building blocks for molecular sieving membranes, *Science*, 2014, **346**, 1356–1359.
10 H. Li, L. Han, J. Hou, J. Liu and Y. Zhang, Oriented zeolitic imidazolate framework membranes within polymeric matrices for effective N_2/CO_2 separation, *J. Membr. Sci.*, 2019, **572**, 82–91.
11 M. S. Denny, J. C. Moreton, L. Benz and S. M. Cohen, Metal–organic frameworks for membrane-based separations, *Nat. Rev. Mater.*, 2016, **1**, 16078.
12 H. B. Park, J. Kamcev, L. M. Robeson, M. Elimelech and B. D. Freeman, Maximizing the right stuff: The trade-off between membrane permeability and selectivity, *Science*, 2017, **356**, eaab0530.
13 A. Felix Sahayaraj, H. Joy Prabu, J. Maniraj, M. Kannan, M. Bharathi, P. Diwahar and J. Salamon, Metal-organic frameworks (MOFs): The next generation of materials for catalysis, gas storage, and separation, *J. Inorg. Organomet. Polym. Mater.*, 2023, **33**, 1757–1781.
14 S. K. B., K. Aswini, A. K. Rao, K. Alam, M. S. Mashkour and A. Jain, Fabrication and characterization of nanoscale metal-organic frameworks (MOFs) for gas storage and separation, *E3S Web Conf.*, 2023, **430**, 01124.
15 M. Martos and I. M. Pastor, Node modification of metal-organic frameworks for catalytic applications, *ChemistryOpen*, 2025, e202400428.

16 S. Zhang, M. Wang, X. Wang, J. Song and X. Yang, Electrocatalysis in MOF films for flexible electrochemical sensing: A comprehensive review, *Biosensors*, 2024, **14**, 420.
17 K. S. Park, Z. Ni, A. P. Côté, J. Y. Choi, R. Huang, F. J. Uribe-Romo, H. K. Chae, M. O'Keeffe and O. M. Yaghi, Exceptional chemical and thermal stability of zeolitic imidazolate frameworks, *Proc. Natl. Acad. Sci. U. S. A.*, 2006, **103**, 10186–10191.
18 G. Chen, G. Liu, Y. Pan, G. Liu, X. Gu, W. Jin and N. Xu, Zeolites and metal–organic frameworks for gas separation: The possibility of translating adsorbents into membranes, *Chem. Soc. Rev.*, 2023, **52**, 4586–4602.
19 F. Şahin, B. Topuz and H. Kalıpçılar, Synthesis of ZIF-7, ZIF-8, ZIF-67 and ZIF-L from recycled mother liquors, *Microporous Mesoporous Mater.*, 2018, **261**, 259–267.
20 Z.-X. Low, J. Yao, Q. Liu, M. He, Z. Wang, A. K. Suresh, J. Bellare and H. Wang, Crystal transformation in zeolitic-imidazolate framework, *Cryst. Growth Des.*, 2014, **14**, 6589–6598.
21 J. K. Zaręba, M. Nyk and M. Samoć, Co/ZIF-8 heterometallic nanoparticles: Control of nanocrystal size and properties by a mixed-metal approach, *Cryst. Growth Des.*, 2016, **16**, 6419–6425.
22 H. T. Kwon, H.-K. Jeong, A. S. Lee, H. S. An and J. S. Lee, Heteroepitaxially grown zeolitic imidazolate framework membranes with unprecedented propylene/propane separation performances, *J. Am. Chem. Soc.*, 2015, **137**, 12304–12311.
23 A. D. Burrows, Mixed-component metal–organic frameworks (MC-MOFs): Enhancing functionality through solid solution formation and surface modifications, *CrystEngComm*, 2011, **13**, 3623–3642.
24 S. Furukawa, K. Hirai, Y. Takashima, K. Nakagawa, M. Kondo, T. Tsuruoka, O. Sakata and S. Kitagawa, A block PCP crystal: Anisotropic hybridization of porous coordination polymers by face-selective epitaxial growth, *Chem. Commun.*, 2009, 5097–5099.
25 T. T. Y. Tan, J. T. M. Cham, M. R. Reithofer, T. S. Andy Hor and J. M. Chin, Motorized Janus metal organic framework crystals, *Chem. Commun.*, 2014, **50**, 15175–15178.
26 S. Y. Toru Wakihara, K. Iezumi and T. Okubo, Heteroepitaxial growth of a zeolite film with a patterned surface-texture, *J. Am. Chem. Soc.*, 2003, **125**, 12388–12389.
27 H.-K. Jeong, J. Krohn, K. Sujaoti and M. Tsapatsis, Oriented molecular sieve membranes by heteroepitaxial growth, *J. Am. Chem. Soc.*, 2002, **124**, 12966–12968.
28 X. Zeng, W. Zhou, P. Zhou, M. Zhang, C. Zhou, L. Tan and L. Wang, ZIF-L(Co) coated stainless steel meshes with superwettability for efficient multiphase liquid separation, *J. Environ. Chem. Eng.*, 2021, **9**, 105325.
29 S. Mo, Q. Zhang, Q. Ren, J. Xiong, M. Zhang, Z. Feng, D. Yan, M. Fu, J. Wu, L. Chen and D. Ye, Leaf-like Co-ZIF-L derivatives embedded on Co_2AlO_4/Ni foam from hydrotalcites as monolithic catalysts for toluene abatement, *J. Hazard. Mater.*, 2019, **364**, 571–580.
30 L. Yang, Z. Wang and J. Zhang, Highly permeable zeolite imidazolate framework composite membranes fabricated *via* a chelation-assisted interfacial reaction, *J. Mater. Chem. A*, 2017, **5**, 15342–15355.
31 J. Yan, T. Ji, Y. Sun, S. Meng, C. Wang and Y. Liu, Room temperature fabrication of oriented Zr-MOF membrane with superior gas selectivity with zirconium-oxo cluster source, *J. Membr. Sci.*, 2022, **661**, 120959.
32 K. Yang, S. Hu, Y. Ban, Y. Zhou, N. Cao, M. Zhao, Y. Xiao, W. Li and W. Yang, ZIF-L membrane with a membrane-interlocked-support composite architecture for H_2/CO_2 separation, *Sci. Bull.*, 2021, **66**, 1869–1876.